wall jet flow exists; and at $Re\, g_w = 4$, $\sqrt{(Re/S_a)}g_w^2 = 0.08$, the free jet exists. For the vortex flow the scaling region is approximately the same for both types of forcing, suggesting that the scaling is not dependent on the type of forcing used in this study.

Figures 3 and 4 depict the phase-averaged velocity fields for the actuator operating in the vortex mode. Each figure represents the average of 10 samples at a particular phase of the actuator plate oscillation. As seen, a vortex structure is measured above the piston for each phase suggesting that the structure is stationary; note that similar results are observed for the additional six phases not presented. This trend is consistent with the averaged flow-visualization pattern and computations.[7] In addition, an unsteady angled jet flow is pumped from the wide gap, which is indicative of mass ejection from the actuator. Each of the phase-averaged velocity fields were averaged to compute the mean flowfield. This result (not presented) indicates that a single cell vortex is generated from the actuator and also verifies the stationarity of the vortex.

Concluding Remarks

A parameter study of the stand-alone JaVA has been implemented for the vortex flowfield. The actuator plate size and forcing were varied to change the strength of the actuator-induced vortex. Measurements indicated that the vortex strength increases with driver repetition rate for a fixed wide slot and plate width. For a fixed driver repetition rate and wide-slot to plate-width ratio, the vortex strength increased as the plate width decreased with only a relatively small decrease in core vortex size. Using an asymmetric plate driver, a stronger vortex is generated for the same actuator geometry and driver repetition rate; however, this trend needs to be verified at higher frequencies. The phase-locked velocity measurements indicated that the vortex structure is stationary and (expectantly) shows unsteadiness near the wide-slot opening. Both of these results are consistent with earlier computations. The nondimensional scaling for the actuator was determined and provided an operating range for the actuator in different flow regimes. When placed in a turbulent boundary layer, the actuator (operated in the vortex regime) can potentially be used to generate streamwise vortices to control flow separation. When operated in the wall regime, the actuator could potentially be used to locally accelerate a boundary-layer flow.

Acknowledgments

This work was performed while the first author held a National Research Council Post-Doctoral Fellowship at NASA Langley Research Center. This work was supported by the Aircraft Morphing element of the NASA Airframe Systems Program Office and by the Air Force Office of Scientific Research.

References

[1]Wiltse, J. M., and Glezer, A., "Manipulation of Free Shear Flows Using Piezoelectric Actuators," *Journal of Fluid Mechanics*, Vol. 249, 1993, pp. 261–285.

[2]Amitay, M., Smith, B. L., and Glezer, A., "Aerodynamic Flow Control Using Synthetic Jet Technology," AIAA Paper 98-0208, Jan. 1998.

[3]Compton, D. A., and Johnston, J. P., "Streamwise Vortex Production by Pitched and Skewed Jets in a Turbulent Boundary Layer," *AIAA Journal*, Vol. 30, No. 3, 1992, pp. 640–647.

[4]Lachowicz, J. T., Yao, C., and Wlezien, R. W., "Scaling of an Oscillatory Flow Control Actuator," AIAA Paper 98-0330, Jan. 1998.

[5]Lachowicz, J. T., Yao, C., and Wlezien, R. W., "Flow Field Characterization of a Jet and Vortex Actuator," *Experiments in Fluids*, Vol. 26, 1999, pp. 12–20.

[6]Jacobson, S. A., and Reynolds, W. C., "Active Control of Streamwise Vortices and Streaks in Boundary Layers," *Journal of Fluid Mechanics*, Vol. 360, 1998, pp. 179–212.

[7]Joslin, R. D., Lachowicz, J. T., and Yao, C., "DNS of Flow Induced by a Multi-Flow Actuator," American Society of Mechanical Engineers, Paper FEDSM98-5302, June 1998.

Sensing Aircraft Icing Effects by Unsteady Flap Hinge-Moment Measurement

Holly M. Gurbacki* and Michael B. Bragg†
University of Illinois at Urbana–Champaign, Urbana, Illinois 61801

Introduction

ICE-INDUCED flow separation can lead to severe performance degradation and reduced aircraft control effectiveness. Trunov and Ingelman-Sundberg[1] demonstrated the effects of ice and roughness on the hinge moment of a tailplane. For the clean, no-ice case the hinge-moment coefficient C_h increased linearly with negative angle of attack until rising sharply at stall. The nonlinearity was the result of flow separation from the lower tailplane surface, where the control surface was abruptly sucked downward as a result of decreased pressure. With ice or roughness at the leading edge, the break in the linear curve occurred at a smaller, less negative angle, and the increase in C_h was less abrupt, eventually leveling out after tailplane stall. Separated flow over a control surface can also lead to reduced control effectiveness. This effect was known as far back as 1940 when Johnson[2] measured a 40% reduction in roll authority as a result of the presence of ice.

Problems such as the increased magnitude in hinge moment and the loss of control effectiveness may have led to a number of ice-related aircraft accidents.[3] It is suspected that the ATR-72 commuter aircraft flight 4184 that crashed on 31 October 1994 in Roselawn, Indiana, is one such example. Bragg[4] studied the effects of supercooled large droplets (SLD) icing conditions on aircraft control and speculated as to the cause of the ATR incident. An ice ridge located aft of the upper surface deicing boot can result from the presence of SLD in the atmosphere and can have a detrimental effect on the lateral control of the aircraft.

Although the pilot and crew may be conscious of the presence of ice on the aircraft, they may be completely unaware of the severity of the icing condition and its effects on aircraft performance and handling qualities. In an effort to identify an easily measurable quantity lying at the source of the ice-induced unsteady separated flowfield, the rms flap hinge-moment coefficient was examined. Experimental results showed that the time-dependent hinge-moment coefficient indicated unsteadiness in the flowfield while the airfoil lift coefficient was still in the linear range. As the angle of attack was increased, a significant increase in the parameter occurred, clearly distinguishing the simulated-iced airfoil from the clean airfoil. The initial change in the time-dependent parameter always took place before the nonlinearity in the steady-state hinge moment, which occurred before the flowfield completely separated. The unsteady hinge-moment coefficient proved to be a viable warning of imminent performance and control degradation. The purpose of this Note is to describe these results in more detail.

Results and Discussion

Experiments were performed in a conventional 3×4 ft (91.44×121.92 cm) indraft, open-return, low-turbulence wind tunnel. The airfoil model was an 18-in. (45.72 cm) chord modified NACA 23012

Received 29 November 2000; revision received 5 January 2001; accepted for publication 25 January 2001.

*Graduate Research Assistant, Department of Aeronautical and Astronautical Engineering, 306 Talbot Lab, 104 S. Wright Street.

†Professor and Head, Department of Aeronautical and Astronautical Engineering, 306 Talbot Lab, 104 S. Wright Street.

(referred to as 23012m) with a 25% chord simple flap. In comparison to a conventional 23012 airfoil, the model had a slightly drooped leading edge and a maximum thickness of 12.2% (see Ref. 5). The simulated ice accretion used in the experiment was a forward-facing, quarter round of 0.25-in. (0.635 cm) radius. The simulated ice was placed on the airfoil model at locations of $x/c = 0.02, 0.10$, and 0.20, and the tests were performed at a Reynolds number of 1.8×10^6 and Mach number of 0.18. A more detailed description of the experiment can be found in Refs. 5–8.

Aerodynamic performance coefficients were calculated from both force-balance data and integrated surface pressure measurements according to standard definitions. The flap hinge moment was determined from a load cell located within a two-arm linkage attached to the flap spar, which was used for actuation of the control surface. The C_h was obtained by determining the trailing-edge down moment about the flap hinge line and nondimensionalized by the flap chord length and surface area. Unsteady C_h measurements were taken at 3000 Hz for angles of attack α less than zero deg and 2000 Hz for angles of zero deg or greater. A total of 10,000 samples were taken for each unsteady measurement. The results were expressed in the form of the rms of the C_h, given by the conventional definition

$$C_{h,\mathrm{rms}} = \sqrt{\frac{1}{N}\sum (C_h - \overline{C_h})^2}$$

where $N = 10{,}000$. All aerodynamic coefficients were corrected for wall effects using the method described by Barlow et al.[9] Uncertainties were calculated based on the iced case at a 5° angle of attack and zero flap deflection. The reported lift coefficient is based on the pressure measurements and has an uncertainty of 0.59% while the hinge-moment coefficient calculated from load cell measurements has an uncertainty of 11.8%. This higher percentage is caused by the small values of the measured hinge moments at $\alpha = 5$ deg.

Because of flow separation induced by the quarter-round ice simulation, the simulated-iced airfoil exhibited remarkably different performance characteristics than the clean case. As illustrated in Fig. 1, the maximum lift coefficient $C_{\ell\,\max}$ and the angle of attack at which it occurred were significantly reduced. Furthermore, fluorescent-oil flow visualization provided evidence that the stall type changed from the characteristic leading-edge stall of the clean NACA 23012m to that of a thin-airfoil-type stall for the simulated-iced airfoil.

Trends in the hinge-moment coefficient were similar to those found by Trunov and Ingelman-Sundberg[1] and are shown in Fig. 2. For the clean airfoil the significant change (or break) in C_h occurred at an angle of attack more than twice that of the simulated-iced cases. This angle was determined by calculating second-order, forward and backward first derivatives based on a total of five data points at a given angle. The percentage difference between the two values was the greatest when there existed a significant change in the slope, corresponding to the break in the C_h curve. Flow visualization revealed that this change in hinge moment corresponded to the reattachment location of the separation bubble reaching the flap.[8] The solid symbols in the figure denote the angles corresponding to the linear lift range (Fig. 1) associated with each case. Thus, the C_h break always occurred in the nonlinear region of the lift curve. Also indicated in the figure were the angles at which $C_{\ell\,\max}$ and complete upper surface flow separation occurred. Both took place after the hinge-moment break.

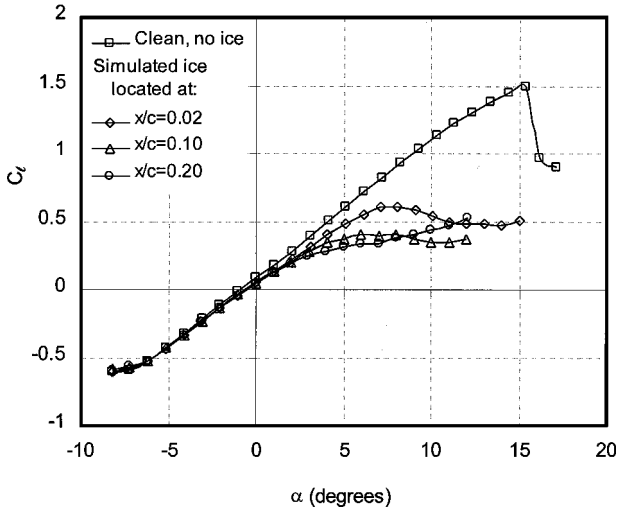

Fig. 1 Lift coefficient for the clean and simulated-iced airfoil at three ice-shape locations.

Table 1 Angle-of-attack locations of significant flowfield events for the clean and simulated-iced airfoil at three ice-shape locations

Ice location	$C_{h,\mathrm{rms}}$ break, deg	C_h break, deg	Separation, deg	$C_{\ell,\max}$, deg
Clean	16.4	16.4	16.4	15.4
$x/c = 0.02$	5	7	8	8
$x/c = 0.10$	−2	3	5	6
$x/c = 0.20$	−3	1	3	6

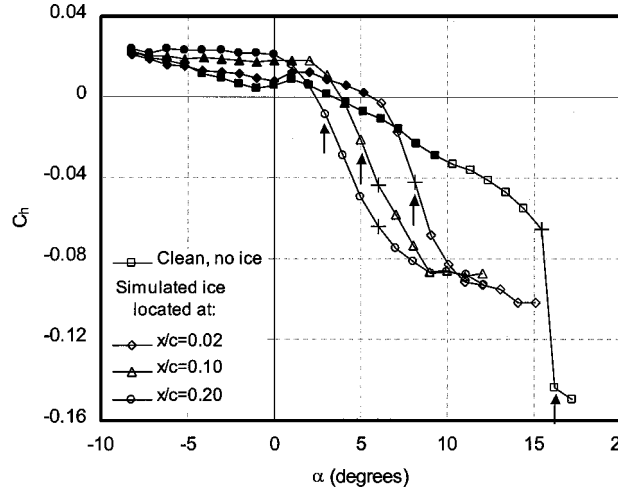

Fig. 2 Steady-state hinge-moment coefficient for the clean and simulated-iced airfoil at three ice-shape locations. Corresponding linear lift-curve regions for each case are denoted by ▲, ●, ■, whereas △, ○, □ represent the nonlinear regions. Arrows represent the angle at which the upper surface flowfield was completely separated, and + denote the location of maximum lift.

These results show that because of the leading-edge stall of the clean airfoil, $C_{\ell\,\max}$ and the abrupt flowfield separation over the entire upper surface of the model occurred almost simultaneously, causing significant reduction in hinge moment. In contrast, separation on the iced airfoil was a gradual process. The flow separated from the simulated ice and reattached further aft on the upper surface. With increasing angle of attack, reattachment moved progressively downstream. It reached the flap (initiating the decline in C_h), eventually moved to the trailing edge (causing complete flow separation) and was followed by, or corresponded to maximum lift. The specific angles of attack at which these events occurred are listed in Table 1.

The comparison of clean and simulated-iced results of the unsteady hinge moment is shown in Fig. 3. For the clean airfoil $C_{h,\mathrm{rms}}$ remained fairly constant throughout the entire angle of attack range until stall. The abrupt increase in $C_{h,\mathrm{rms}}$ coincided with the upper surface flowfield separation, $C_{\ell\,\max}$ and the hinge-moment reduction. With the quarter-round ice simulation present, the break in $C_{h,\mathrm{rms}}$ (or departure from the clean case) was more gradual and occurred at decreased angles of attack. Table 1 lists the exact angles of the breaks, which were determined to occur when the simulated-iced

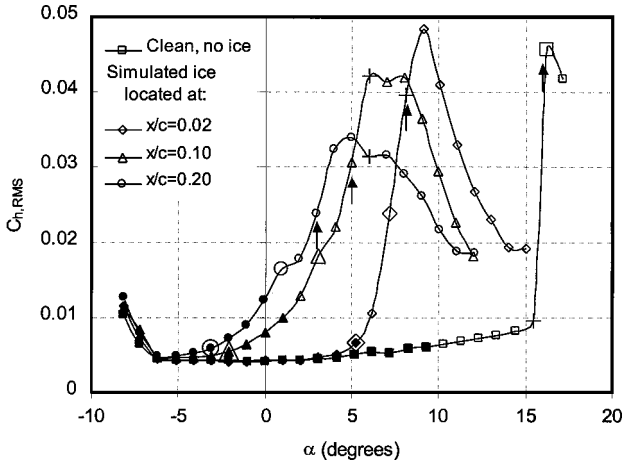

Fig. 3 Unsteady rms hinge-moment coefficient for the clean and simulated-iced airfoil at three ice-shape locations. Corresponding linear lift-curve regions for each case are denoted by ▲, ●, ■, whereas △, ○, □ represent the nonlinear regions. The outlined symbols of the simulated-iced cases denote the locations of the $C_{h,\mathrm{rms}}$ break. The enlarged symbols indicate the angle at which the C_h break occurred, and ↑ represent the angle at which the upper surface flowfield was completely separated. The + denote the location of maximum lift.

$C_{h,\mathrm{rms}}$ values were 30% greater than the clean airfoil values at corresponding angles of attack.

The $C_{h,\mathrm{rms}}$ breaks of the simulated-iced airfoil occurred in the linear lift-curve regions, apparent from the solid symbols in the figure. Evidence suggests that the increasing unsteadiness of the ice-induced separation bubble caused an increase in $C_{h,\mathrm{rms}}$ before the rapid bubble growth caused a nonlinearity in C_ℓ. The rise in the unsteady parameter served as a precursor to several subsequent flowfield events. In each simulated-iced case, as the angle of attack increased, the $C_{h,\mathrm{rms}}$ broke from the clean airfoil values and was followed by a break in C_h, complete upper surface flow separation, and finally $C_{\ell\,\max}$. Table 1 shows that the break in $C_{h,\mathrm{rms}}$ occurred approximately 2–4 deg before the C_h break and 3–9 deg before $C_{\ell\,\max}$ was reached.

Conclusions

The rms hinge-moment coefficient provides a clear distinction between clean and simulated-iced airfoils even before the nonlinear-lift range is reached. Simulated-iced $C_{h,\mathrm{rms}}$ values differ significantly from those of the clean case before the C_h break (when flow reattachment reaches the flap) and prior to flow separation over the entire airfoil surface.

If the pilot were to have access to unsteady hinge-moment data during flight, a notable departure from the expected clean values could provide warning of performance and control degradation. Rather than relying on the maximum control surface deflection or stall angle based on the clean airfoil case, the pilot could be alerted to possible flap and angle of attack restrictions derived from real-time performance monitoring based on this rms hinge-moment parameter.

Acknowledgments

This work was supported in part by a Critical Research Initiatives Grant from the University of Illinois at Urbana–Champaign. The authors would also like to thank the Federal Aviation Administration Technical Center for the use of the NACA 23012m airfoil model, and Andy Broeren and Sam Lee at Illinois for their assistance.

References

[1]Trunov, O. K., and Ingelman-Sundberg, M., "On the Problem of Horizontal Tail Stall Due to Ice," Swedish-Soviet Working Group on Scientific-Technical Cooperation in the Field of Flight Safety, The Swedish Board of Civil Aviation and USSR Ministry of Civil Aviation, Moscow, Rept. JR-3, Feb. 1985.

[2]Johnson, C. L., "Wing Loading, Icing and Associated Aspects of Modern Transport Design," *Journal of the Aeronautical Sciences*, Vol. 8, No. 2, 1940, pp. 43–54.

[3]Bradley, J. J., "A Safety and Economics Study of Aircraft Ice Protection," M.S. Thesis, Dept. of Aeronautical and Astronautical Engineering, Univ. of Illinois at Urbana–Champaign, IL, Aug. 1999.

[4]Bragg, M. B., "Aircraft Aerodynamic Effects due to Large Droplet Ice Accretions," AIAA Paper 96-0932, Jan. 1996.

[5]Lee, S., Dunn, T., Gurbacki, H. M., Bragg, M. B., and Loth, E., "An Experimental and Computational Investigation of Spanwise-Step-Ice Shapes on Airfoil Aerodynamics," AIAA Paper 98-0490, Jan. 1998.

[6]Lee, S., and Bragg, M. B., "Effects of Simulated-Spanwise Ice Shapes on Airfoils: Experimental Investigation," AIAA Paper 99-0092, Jan. 1999.

[7]Lee, S., and Bragg, M. B., "Experimental Investigation of Simulated Large-Droplet Ice Shapes on Airfoil Aerodynamics," *Journal of Aircraft*, Vol. 36, No. 5, 1999, pp. 844–850.

[8]Gurbacki, H. M., "Sensing Aircraft Icing Effects from Flap Hinge-Moment Measurement," M.S. Thesis, Dept. of Aeronautical and Astronautical Engineering, Univ. of Illinois at Urbana–Champaign, IL, May 2000.

[9]Barlow, J. B., Rae, W. H., and Pope, A., "Boundary Corrections I: Basics and Two-Dimensional Cases," *Low-Speed Wind Tunnel Testing*, 3rd ed., Wiley, New York, 1999, pp. 328–366.

Flow Quality Improvements in a Blowdown Wind Tunnel

H. Sundara Murthy,* R. S. Verma,*
S. P. Jagadeeswarachar,* and Rajan Kumar*
National Aerospace Laboratories,
Bangalore 560 017, India

Introduction

A HIGH level of flow unsteadiness in wind tunnels is undesirable because it can influence certain aerodynamic phenomena, such as the location of boundary-layer transition and subsequent growth of the turbulent boundary layer on models. It can also lead to problems in carrying out or can even impede certain dynamic measurements in the tunnel. Although flow unsteadiness is a generic term covering velocity fluctuations (turbulence), pressure fluctuations (acoustic noise), and temperature (entropy) fluctuations in freestream, acoustic noise is usually dominant in conventional subsonic/transonic tunnels and flow unsteadiness in wind tunnels is normally assessed by noise level measurements.

Noise levels in the National Aerospace Laboratories (NAL) 1.2-m blowdown wind tunnel were found to be high, which resulted in reduced accuracy of certain dynamic measurements and data interpretation problems. The principal sources of the noise were found to be the pressure regulating valve and the perforated wall test section in the tunnel (see Fig. 1a). To overcome these problems a major refurbishment program aimed at reducing the high noise levels in the tunnel was undertaken. The goal was to reduce the pressure fluctuation coefficient Cp_{rms} (equal to $\bar{P}/q$, where $\bar{P}$ is the rms static pressure fluctuation in the test section and q is the freestream dynamic pressure) to $\leq 1\%$ in the subsonic and transonic speed regime and $\leq 0.2\%$ at supersonic speeds. This Note presents brief details of the modifications incorporated and the results of wind-tunnel tests conducted to evaluate the flow quality improvements achieved.

Details of Modification

A relative assessment of different concepts tried elsewhere indicated that installation of acoustic baffles in the settling chamber

Received 19 October 2000; revision received 31 January 2001; accepted for publication 1 February 2001.

*Scientist, National Trisonic Aerodynamic Facilities.